Digest Journal of Nanomaterials and Biostructures Vol. 17, No. 4, October-December 2022, p. 1527-1533

Structural, optical and electrical impacts of Ni^{2+} on $Mg_{1-x}Fe_{1.9}Sm_{0.1}O_4$ (x = 0.0, 0.2, 0.4 and 0.6) spinel ferrites

M. S. Hasan[a], M. I. Khan[a,*], S. Kanwal[a], M. I. Irfan[b], Tahani I. Al-Muhimeed[c], S. Mumtaz[d]
[a]*Department of Physics, The University of Lahore, 53700, Pakistan*
[b]*Department of Chemistry, University of Sargodha, Pakistan*
[c]*Department of Chemistry, College of Science, King Saud University, P.O. Box 22452, Riyadh 11451, Saudi Arabia*
[d]*Electrical and Biological Physics, Kwangwoon University, Seoul, 01897, South Korea*

Sol-gel auto combustion was used to create a sequence of soft ferrites, $Ni_xMg_{1-x}Fe_{1.9}Sm_{0.1}O_4$(x = 0.0, 0.2, 0.4 & 0.6). The XRD, FTIR, UV-vis, & four probe I-V techniques, respectively, were used to evaluate the structural, optical, and electrical properties. The cubic crystal structure was confirmed by the XRD pattern. The range of 25.71 - 33.67 nm was found to be the average crystallite size. FTIR spectra provided evidence of the tetrahedral band's existence. With the enhancement of Ni^{2+} concentration, Eg was determined from 2.28-3.21 eV. It was confirmed by the ranges of DC electrical resistivity that materials might be used in transformers to lessen eddy current losses.

(Received July 3, 2022; December 21, 2022)

Keywords: Soft ferrites, FTIR, band gap energy, electrical resistivity

1. Introduction

Due to their substantial electronic, optical, electrical, and magnetic properties, spinel nanoferrites are notable nanomaterials [1-7]. $[M^{2+}][Fe^{3+}]O^{2-}{}_4$, usual molecular formula for spinel soft ferrites is $O_2{}^{-4}$, where M^{2+} is any divalent cation, such as Mg^{2+}, Ni^{2+}, Cd^{2+}, Zn^{2+}, or Mn^{2+}. M^{2+} and Fe^{3+} of FCC lattice, which is sculpted by ions of oxygen in the regular spinel lattice, respectively, occupy the tetrahedral [A] & octahedral [B] interstitial sites [8]. These materials have attained the attentions of scientists due to wonderful applications. $NiFe_2O_4$ exibits structure of inverse spinel [9]. But when magnetic moments at low temperature are smaller than the bulk materials and also the crystallite size is reduced to nanometer range it shows mixed spinel structure [10]. The variation in coordination of A and B sites or cations redistributions leads the deviation in $NiFe_2O_4$ from inverse to mixed spinel structures [11]. So, Ni2+ & Fe3+ ions occupies both A & B interstitial spaces in the $NiFe_2O_4$ structure [12]. Such types of soft ferrites are applicable in various fields like catalysis, ferro-fluids, microwave, gas sensors, medical, optical and magnetic devices [13-18]. Magnetic interactions & cation distributions at interstitial sites are related to the structural & magnetic characteristics of spinel ferrites. Mg2+ occupies 45% of the A site and 55% of the B site and has a partial spinel structure. Small proportion of rare earth metal (Sm^{3+}) is added in octahedral site to improve the structural, optical and electrical properties [19]. Various techniques are employed to synthesize nanoferrites including microwave refluxing, hydrothermal, co-precipitation, citrate gel, sol-gel, spray pyrolysis etc., [13, 15, 16, 20]. The proper application of synthesis process is associated to desire outcomes and applications of composed materials. Among the most widely used and cost-effective methods is sol-gel auto-combustion. Due to its simplicity and ability to regulate grain size, it is appropriate. Spinel ferrites with $Ni_xMg_{1-x}Fe_{1.9}Sm_{0.1}O_4$(x = 0.0, 0.2, 0.4, & 0.6) were manufactured in the current research to examine their structural, optical & electrical properties.

* Corresponding author: muhammad.iftikhar@phys.uol.edu.pk
https://doi.org/10.15251/DJNB.2022.174.1527

2. Synthesis and characterizations of $Ni_xMg_{1-x}Fe_{1.9}Sm_{0.1}O_4$

By using the sol-gel auto combustion process, a series of soft nanoferrites made of $Ni_xMg_{1x}Fe_{1.9}Sm_{0.1}O_4$ (x = 0.0, 0.2, 0.4 & 0.6) were created. According to stoichiometric ratios, nickel nitrate(Ni(NO3)2.4H2O_4), magnesium nitrate(Mg(NO3)2.6H2O_4), iron nitrate($Fe(NO_3)_2.9H_2O$), and samarium nitrate($Sm(NO_3)_3.6H_2O$) were taken. By taking proportion (1/1.2) of nitrates and citric acid, were added into deionized water. They were dissolved with the help of magnetic stirrer. The pH was maintained 7 or 8 via the drop-wise addition of ammonia solution. The dry gel obtained at 80℃ during unstopped stirring of one hour. After the formation of dry gel only the heat was provided and the product in form of nanoparticles was achieved through auto-combustion. The obtained product was grinded to attain fine powder. Finally, the muffle furnace was used to anneal the particles at 800℃ for 8 hours. Various characterizations like FTIR, XRD, UV-vis and I-V four probe were adapted to determine structural, optical and electrical properties of nanomaterials, respectively.

3. Structural properties

The XRD patterns of nanoferrite particles with compositional formula $Ni_xMg_{1-x}Fe_{1.9}Sm_{0.1}O_4$ (x = 0.0, 0.2, 0.4 and 0.6) are shown in Figure 1. All samples showed single phase crystals and (220), (311), (422) and (511) were most prominent peaks. The average crystallite (D) size was calculated using Scherrer's formula [21],

$$D = \frac{0.9\lambda}{\beta cos\theta} \tag{1}$$

where FWHM stands for full width at half maximum, λ is 1.542 Å for the angle of Bragg. The measured values of usual crystallite size are illustrated in Table 1. The equation as was used to determine the lattice constant and the volume of the unit cell [22],

$$a = d\sqrt{h^2 + k^2 + l^2} \tag{2}$$

$$d = \frac{n\lambda}{2sin\theta} \tag{3}$$

$$V = a^3 \tag{4}$$

where h, k, & l are Miller indices and d is the dislocation line density. Table 1 displays the computed lattice constant values. Figure 2 demonstrates the relation between lattice constant & average crystallite size contrary to Ni^{2+} concentration. The graphic shows that the average crystallite size increases as the quantity of Ni^{2+} rises. Due to the difference in radii between Mg^{2+} (0.72 Å) & Ni^{2+} (0.69 Å), it does seem that the lattice constant decreases as the concentration of Ni2+ increases. As smaller ionic radii take the place of greater ionic radii [19]. Additionally, the relations as follows were used to estimate the X-ray density (dx) as well as bulk density (d_b).

$$d_x = \frac{ZM_w}{VN_A} \tag{5}$$

$$d_b = \frac{m}{\pi r^2 h} \tag{6}$$

where Z is 8, Mw are the molecular weights of the composite samples, V are the volumes of the unit cells, N_A are Avogadro's numbers, r are the radii of the nanoferrite pellets, and h are their thicknesses. Table 1 presents the reported values of dx & db.

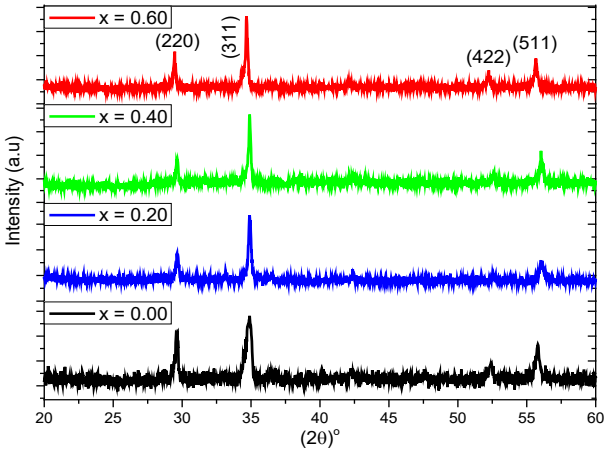

Fig. 1. XRD patterns of $Ni_xMg_{1-x}Fe_{1.9}Sm_{0.1}O_4$(x = 0.0, 0.2, 0.4 and 0.6) soft ferrite.

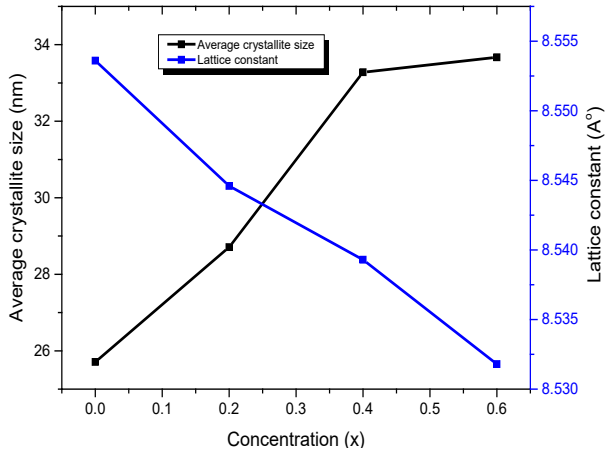

Fig. 2. Lattice constant (a) &Average crystallite size (D) for$Ni_xMg_{1-x}Fe_{1.9}Sm_{0.1}O_4$ (x = 0.0, 0.2, 0.4, and 0.6) soft ferrites are correlated with concentrations.

Table 1. $Ni_xMg_{1-x}Fe_{1.9}Sm_{0.1}O_4$(x = 0.0, 0.2, 0.4, and 0.6) soft ferrites: compositions, crystallite size (D), lattice parameter (a), volumes of unit cells (V), X-ray density (dx), and bulk density (db).

x	Composition	D (nm)	a (Å)	V $(Å)^3$	D_x $(g.cm^{-3})$	d_b $(g.cm^{-3})$
0.0	$Mg_1Fe_{1.9}Sm_{0.1}O_4$	25.71	8.5536	625.81	4.4458	3.5388
0.2	$Ni_{0.2}Mg_{0.8}Fe_{1.9}Sm_{0.1}O_4$	28.71	8.5446	623.84	4.6064	3.6550
0.4	$Ni_{0.4}Mg_{0.6}Fe_{1.9}Sm_{0.1}O_4$	33.28	8.5393	622.69	4.7617	3.7712
0.6	$Ni_{0.6}Mg_{0.4}Fe_{1.9}Sm_{0.1}O_4$	33.67	8.5318	621.04	4.9214	3.8875

4. Fourier transform infrared spectroscopy(FTIR)

The distribution of ions on tetrahedral and octahedral sites was determined using FTIR. Figure 3 displays the FTIR spectra of soft ferrites composed of $Ni_xMg_{1-x}Fe_{1.9}Sm_{0.1}O_4$ (x = 0.0, 0.2, 0.4 & 0.6). Fe-O stretching vibrations and the oxygen tetrahedron are linked to the upper frequency band (v_1). The maximum +3 valency is seen in spinel ferrite structures, hence this frequency range is attributed to Fe^{3+}(A/B)O^{2-} vibrations. For x = 0.0 to 0.6, the frequency band ranges for 1 are 539.11 to 545.12 cm^{-1}, respectively. The differences in Fe^{3+}-O_2 bond lengths at the tetrahedral site are thought to be responsible for the changes in band locations[23].

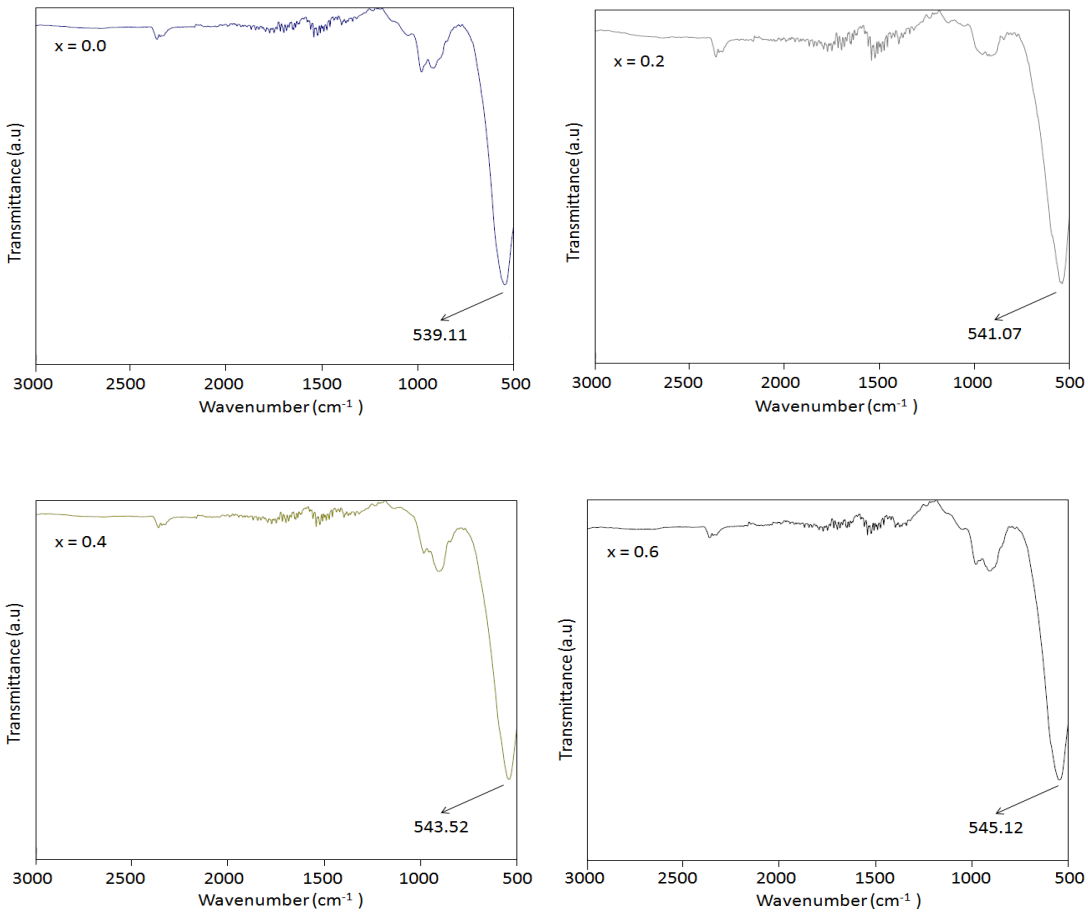

Fig. 3. FTIR spectra of $Ni_xMg_{1-x}Fe_{1.9}Sm_{0.1}O_4$(x = 0.0, 0.2, 0.4 and 0.6) soft ferrites.

Table 2. Tetrahedral absorption band, optical band gap energy and DC electrical resistivity for $Ni_xMg_{1-x}Fe_{1.9}Sm_{0.1}O_4$(x = 0.0, 0.2, 0.4 &0.6) soft ferrite.

X	Absorption band (cm^{-1})	Optical band gap energy, Eg (eV)	DC resistivity (ohm-cm)
0.0	539.11	2.28	5.71 x 10^6
0.2	541.07	2.47	3.63 x 10^7
0.4	542.52	2.89	1.92 x 10^8
0.6	545.12	3.21	9.06 x 10^8

5. UV-visible photometry

To evaluate soft ferrites, UV-visible photometry is a useful method. The absorption coefficient (α) was calculated using the following relationship as,

$$\alpha = 2.303 \frac{\log (A)}{t} \tag{7}$$

where A & t, respectively, stand for absorbance and the length of the light's passage where the absorbance appears. To calculate the optical band gap energy, Tauc's equation is used as,

$$\alpha h\nu = B(h\nu - Eg)^m \tag{8}$$

where m is the number of absorption transition processes and h is Plank's constant, B is the transition probability constant, v is frequency. The optical band gap energy is calculated by plotting (hv) against $(\alpha hv)^2$ as seen in Figure 4, dropping a tangent on the x-axis yields an estimate of the optical band gap energy. Table 2 gives an expression for the optical band gap energy. It can be seen from the tabulated data that optical band gap energy rise as Ni^{2+} ion concentrations rise. Such behaviour might result from a doping ion concentration, the presence of impurities, or surface effects. Additionally, the Eg ranges show that manufactured materials can be used in microwave frequency devices [24].

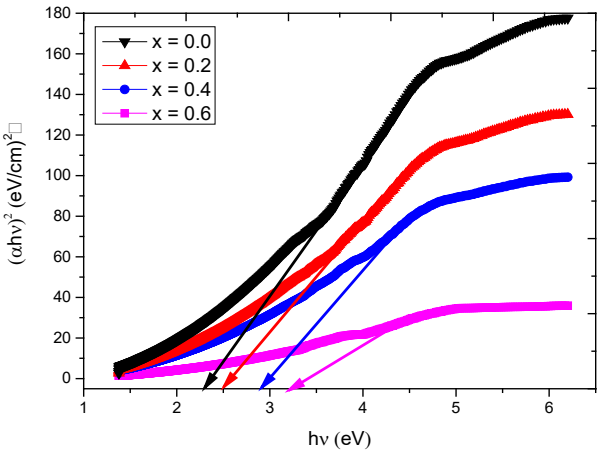

Fig. 4. Tauc's plot for optical band gap energies of $Ni_xMg_{1-x}Fe_{1.9}Sm_{0.1}O_4$(x = 0.0, 0.2, 0.4 and 0.6) soft ferrites.

6. DC electrical resistivity

DC electrical resistivity of Ni^{2+} doped $Mg_{1-x}Fe_{1.9}Sm_{0.1}O_4$ ferrites was determined by using four probe technique at room temperature. In order to calculate the DC resistivity of artificial ferrites, the following relation was used:

$$\rho = \frac{AR}{L} \tag{9}$$

where L & A represent the pellets, thickness & area , respectively. By calculating the inversion of the gradient derived from V and I, one may calculate the resistance R. As shown in Table 2, DC electrical resistivity was found from 5.71×10^6 - 9.06×10^8 ohm-cm for x = 0.0 to 0.6, respectively. Figure 5 depicts the curve of DC resistivity versus concentration. The graph illustrates how resistivity rises as Ni^{2+} concentration does. This behaviour is a result of charge carriers hopping. Such behavior is attributed to hopping of charge carriers. Furthermore, the conductivity of Ni^{2+}(1.43×10^7 S/m) is smaller than the conductivity of Mg^{2+}(2.15×10^7 S/m). Hence, the hopping of charge carriers between the divalent and trivalent iron ions causes the conduction mechanism. So, the reduction in conduction process causes the increase in resistivity with the addition of Ni^{2+} ions [25].

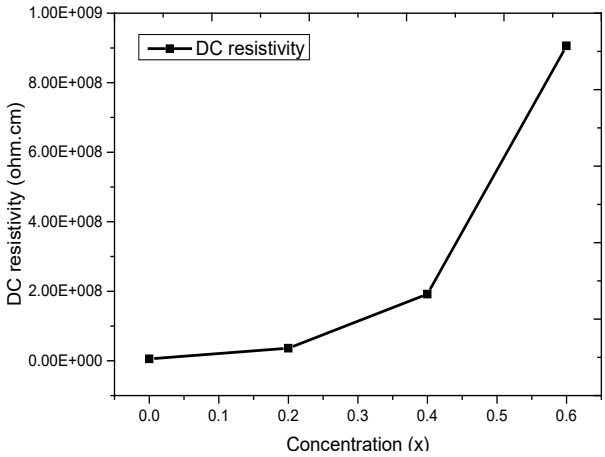

Fig. 5. DC electrical resistivity versus concentration for $Ni_xMg_{1-x}Fe_{1.9}Sm_{0.1}O_4$(x = 0.0, 0.2, 0.4 & 0.6) soft ferrites'.

6. Conclusion

Mg-Fe-Sm soft ferrites were produced using the sol-gel auto combustion process and nickel doped. Composed nanoferrites are in the range of 8.5536 to 8.5318 A°. Various structural parameters were determined by using XRD data. FTIR spectra verified the presence of metal oxides. For soft ferrites, the optical bandgap was expressed by UV-vis spectroscopy. Soft ferrites have a determined DC electrical resistivity of ohm.cm and are a preferred candidate for transformers to lower eddy current losses.

Acknowledgement

The authors extend their appreciation to the Researchers Supporting Project number (RSP-2021/394) King Saud University, Riyadh, Saudi Arabia.

References

[1] ALI, I., et al., Digest J. Nanomater. Biostruct, 2020. 15.

[2] Amin, N., et al., Digest Journal of Nanomaterials and Biostructures, 2019. 14(2): p. 501-507.

[3] Dube, G. and V. Darshane, Journal of molecular catalysis, 1993. 79(1-3): p. 285-296; https://doi.org/10.1016/0304-5102(93)85108-6

[4] Hussain, K., et al., Dig. J. Nanomater. Biostruct., 2019. 14: p. 85-92.

[5] Reddy, C., S. Manorama, and V. Rao, Journal of materials science letters, 2000. 19(9): p. 775-778; https://doi.org/10.1023/A:1006716721984

[6] Reddy, C.G., S. Manorama, and V. Rao, Sensors and Actuators B: Chemical, 1999. 55(1): p. 90-95; https://doi.org/10.1016/S0925-4005(99)00112-4

[7] Sugimoto, M., Journal of the American Ceramic Society, 1999. 82(2): p. 269-280; https://doi.org/10.1111/j.1551-2916.1999.tb20058.x

[8] Mo, N., Y.-Y. Song, and C.E. Patton, Journal of applied physics, 2005. 97(9): p. 093901; https://doi.org/10.1063/1.1887834

[9] Šepelák, V., et al., Journal of Magnetism and Magnetic Materials, 2003. 257(2-3): p. 377-386; https://doi.org/10.1016/S0304-8853(02)01279-9

[10] Chinnasamy, C., et al., Physical Review B, 2001. 63(18): p. 184108; https://doi.org/10.1103/PhysRevB.63.184108

[11] Moradmard, H., et al., Journal of Alloys and Compounds, 2015. 650: p. 116-122; https://doi.org/10.1016/j.jallcom.2015.07.269
[12] Jacob, J. and M.A. Khadar, Journal of applied physics, 2010. 107(11): p. 114310; https://doi.org/10.1063/1.3429202
[13] Amin, N., et al., Ceramics International, 2020. 46(13): p. 20798-20809; https://doi.org/10.1016/j.ceramint.2020.05.079
[14] Khan, M., et al., Ceramics International, 2020. 46(16): p. 24844-24849; https://doi.org/10.1016/j.ceramint.2020.06.268
[15] Khan, M., et al., Ceramics International, 2020. 46(17): p. 27318-27325; https://doi.org/10.1016/j.ceramint.2020.07.217
[16] Khana, M., et al., Chalcogenide Letters, 2022. 19(2): p. 75-82; https://doi.org/10.15251/CL.2022.192.75
[17] Nabi, M., et al., Journal of Superconductivity and Novel Magnetism, 2021. 34(7): p. 1813-1822; https://doi.org/10.1007/s10948-020-05588-x
[18] Saqib, M., et al., Journal of Superconductivity and Novel Magnetism, 2021. 34(2): p. 609-616; https://doi.org/10.1007/s10948-020-05746-1
[19] Hasan, M., et al., Materials Research Express, 2018. 6(1): p. 016302; https://doi.org/10.1088/2053-1591/aae3f6
[20] Khan, M.I., et al., Zeitschrift für Physikalische Chemie, 2022. 236(2): p. 155-168; https://doi.org/10.1515/zpch-2020-1635
[21] Khan, M., et al., Materials Chemistry and Physics, 2021. 274: p. 125177; https://doi.org/10.1016/j.matchemphys.2021.125177
[22] Zulqarnain, M., et al., Journal of Alloys and Compounds, 2022. 894: p. 162431; https://doi.org/10.1016/j.jallcom.2021.162431
[23] Sujatha, C., et al., Journal of magnetism and magnetic materials, 2013. 340: p. 38-45; https://doi.org/10.1016/j.jmmm.2013.03.027
[24] Arshad, M.I., et al., Ceramics International, 2022. 48(10): p. 14246-14260; https://doi.org/10.1016/j.ceramint.2022.01.313
[25] Farooq, W.A., et al., Molecules, 2021. 26(5): p. 1399; https://doi.org/10.3390/molecules26051399